SCIENCE CHINA
Physics, Mechanics & Astronomy

• Article •

April 2014 Vol.57 No.4: 753–763
doi: 10.1007/s11433-013-5234-y

Nonlinear spectral-like schemes for hybrid schemes

HE ZhiWei[1], LI XinLiang[2*] & LIANG Xian[2]

[1] *China North Vehicle Research Institute, Beijing 100072, China;*
[2] *State Key Laboratory of High Temperature Gas Dynamics, Institute of Mechanics, Chinese Academy of Sciences, Beijing 100190, China*

Received September 26, 2012; accepted March 26, 2013; published online February 19, 2014

In spectral-like resolution-WENO hybrid schemes, if the switch function takes more grid points as discontinuity points, the WENO scheme is often turned on, and the numerical solutions may be too dissipative. Conversely, if the switch function takes less grid points as discontinuity points, the hybrid schemes usually are found to produce oscillatory solutions or just to be unstable. Even if the switch function takes less grid points as discontinuity points, the final hybrid scheme is inclined to be more stable, provided the spectral-like resolution scheme in the hybrid scheme has moderate shock-capturing capability. Following this idea, we propose nonlinear spectral-like schemes named weighted group velocity control (WGVC) schemes. These schemes show not only high-resolution for short waves but also moderate shock capturing capability. Then a new class of hybrid schemes is designed in which the WGVC scheme is used in smooth regions and the WENO scheme is used to capture discontinuities. These hybrid schemes show good resolution for small-scales structures and fine shock-capturing capabilities while the switch function takes less grid points as discontinuity points. The seven-order WGVC-WENO scheme has also been applied successfully to the direct numerical simulation of oblique shock wave-turbulent boundary layer interaction.

group velocity control, hybrid, WENO, shockwave-turbulent boundary layer interaction, direct numerical simulation

PACS number(s): 47.11.Bc, 47.40.Nm, 47.27.ek

Citation: He Z W, Li X L, Liang X. Nonlinear spectral-like schemes for hybrid schemes. Sci China-Phys Mech Astron, 2014, 57: 753–763, doi: 10.1007/s11433-013-5234-y

Shock wave-turbulent boundary layer interaction (SWTBLI) problems, characterized by turbulences and shockwaves, are archetypical examples of multi-scales problems with discontinuities. Because of the importance and widely applications of these problems [1], direct numerical simulations (DNS) of SWTBLI problems have been required continually.

The multi-scales phenomena in such problems requires the numerical method to be high order and high resolution. To be reliable, a DNS of such flows must resolve these various scales, particularly smaller ones with accuracy in both amplitude and phase [2]. Concerning high-order and high-resolution schemes, there have been upwind compact schemes [3,4], dispersion-relation preserving schemes [5] and wavenumber-extended finite difference schemes [6]. These schemes are all designed for high resolution of short waves with respect to the computational grid. Another high-resolution schemes are explicit/compact central schemes [7] which have no dissipation resulted in providing spurious solutions and leading to inevitable stability problems [8,9].

However, these methods above are limited to compute flows without discontinuities. To capture shocks, treating these methods nonlinearly is required [4]. For flows with discontinuities, WENO [10] schemes which have been demonstrated very promising shock-capturing capabilities and high order accuracy are widely used. However, numerical tests also indicate that classical WENO schemes are usually not optimal for computing turbulent flows or aeroacoustic fields because they are too diffusive for short waves [11].

*Corresponding author (email: lixl@imech.ac.cn)

The observations presented above suggest that, a natural choice is to combine the ENO/WENO scheme with another scheme with spectral-like resolution to form a so-called spectral-like resolution-WENO hybrid scheme [2]. Adams and Shariff [12] have developed hybrid schemes that rely on the coupling of a nonconservative compact upwind scheme with a shock-capturing ENO scheme that is turned on around discontinuities. Pirozzoli [13], following ref. [12], derived a hybrid compact-WENO scheme in which a conservative compact scheme was coupled with a WENO scheme to make the overall scheme conservative. Ren et al. [11] improved the hybrid compact-WENO scheme [11] by removing the abrupt switch between the compact and the shock-capturing schemes through the use of a weighted average of the two schemes. There are still other spectral-like resolution-WENO hybrid schemes [2,14].

However, there are still problems with switch functions in these hybrid schemes. Take the switch function developed by Ren et al. [11] as an example. It was found that this switch function may mistake some points in smooth waves as discontinuity points, particularly in high-wavenumber waves [15]. Thus a problem arises. That is, if the switch function takes more grid points as discontinuity points, the WENO scheme is often turned on, and the numerical solution may be too dissipative. Conversely, if the switch function takes less grid points as discontinuity points, the hybrid schemes usually are found to produce oscillatory solutions or just to be unstable.

Here we propose nonlinear spectral-like schemes with moderate shock capturing capabilities to try to solve this problem. Thus even the switch function takes less grid points as discontinuity points, the new nonlinear spectral-like schemes still be able to withstand this situation because of their moderate shock capturing capabilities. These schemes are based on the group velocity control (GVC) [16, 17] theory. This concept is proposed and used to explain the phenomenon of oscillations near the discontinuities and capture discontinuities [16,17]. The main ideas are that a discontinuity can be treated as a linear combination of long and short waves. Oscillation productions in numerical solution around discontinuities are due to non-uniform group velocity of wavelets. Thus to control group velocities of wavelets could be used to reduce oscillation productions around discontinuities. GVC schemes does be found numerically to have a ability of reducing many oscillations near discontinuities while there still a bit left [17,18].

In this paper, firstly, by following the GVC theory, we propose a weighted methodology of constructing GVC schemes. A new class of schemes named weighted group velocity control (WGVC) schemes is deduced. Then we pay our main attention to show WGVC schemes have high-order and high-resolution property, not to demonstrate their moderate shock-capturing capabilities. Finally, a new class of hybrid schemes is designed in which the WGVC scheme is used in smooth regions while the WENO scheme is used to capture discontinuities. The final hybrid schemes show good resolution for small-scales structures and fine shock-capturing capabilities. And the seven-order WGVC-WENO scheme has also been applied successfully to the DNS of oblique SWTBLI.

1 Group velocity of linear finite difference schemes and WENO schemes

Trefethen [19] surveyed and illustrated the relevance of group velocity to the behavior of finite difference models of time-partial differential equations. For more details on the WENO scheme, refer elsewhere [10]. Here we briefly list these common sense knowledge for completeness.

1.1 Group velocity of linear finite difference schemes

Consider the one-dimensional linear advection equation on an infinite domain with a sinusoidal initial condition with wavenumber κ,

$$\frac{\partial u}{\partial t}+c\frac{\partial u}{\partial x}=0,\ -\infty<x<\infty,\ u(x,0)=\hat{u}_0\mathrm{e}^{\mathrm{i}\kappa x}, \tag{1}$$

where $\mathrm{i}\equiv\sqrt{-1}$ and we assume c=const>0.

Theoretically, applying separation of variables, it is clear that the exact solution to eq. (1) is

$$u(x,t)=\hat{u}_0\mathrm{e}^{\mathrm{i}\kappa(x-ct)}. \tag{2}$$

In practice, eq. (1) is discretized in the spatial domain on a uniform grid with nodes given by $x_j=j\Delta x,\ j=0,...,N$, where Δx is the cell size. To facilitate the discussion, let operator L denote the approximation of the spatial differential, $\dfrac{L(u_j)}{\Delta x}\approx\left.\dfrac{\partial u}{\partial x}\right|_{x=x_j}$. Here we consider an explicit, linear finite difference operator, that is,

$$L(u_j)=\sum_{l=-sl}^{sr}a_l u_{j+l}, \tag{3}$$

where sl and sr are arbitrary positive integers and a_l, $l=-sl,\cdots,sr$ are constant coefficients. Then the semi-discretized form of eq. (1) by the method of lines yields a system of ordinary differential equations

$$\frac{\mathrm{d}u_j}{\mathrm{d}t}+c\frac{L(u_j)}{\Delta x}=0,\ u(0)=\hat{u}_0\mathrm{e}^{\mathrm{i}\kappa x_j},\ j=0,...,N, \tag{4}$$

where $u_j=u(x_j,\ t)$. Then the exact solution to the semi-discrete equation is

$$u(x_j,t)=\hat{u}_0\mathrm{e}^{\mathrm{i}(\kappa x_j-K_e ct)}, \tag{5}$$

where $K_e(\kappa)=\frac{1}{\mathrm{i}\Delta x}\sum_{l=-sl}^{sr} a_l \mathrm{e}^{\mathrm{i}(l\Delta x)}$. For convenience we introduce the reduced wavenumber $\xi=\kappa\Delta x$ [7] and the reduced modified wavenumber $\Xi(\xi)=K_e(\kappa)\cdot\Delta x$ which is a complex number $\mathrm{Re}(\Xi)+\mathrm{i}\,\mathrm{Im}(\Xi)$. Then we can rewrite eq. (5) as:

$$u(x_j,t)=\hat{u}_0\mathrm{e}^{\mathrm{Im}(\Xi)ct/\Delta x}\mathrm{e}^{\mathrm{i}\kappa(x_j-\mathrm{Re}(\Xi)ct/\xi)}. \tag{6}$$

$\mathrm{Im}(\Xi)$ contains information on the spectral dissipation property of the scheme. $\mathrm{Re}(\Xi)$ contains information on the spectral dispersion property of the scheme. Details can be found in refs. [2,4,19].

In ref. [16], group velocity of a this linear difference scheme is defined $\frac{\mathrm{d}}{\mathrm{d}\xi}(\mathrm{Re}(\Xi))$ for constant c. And a new classification for the linear difference operator L is introduced, that is, the operator L: with $\frac{\mathrm{d}}{\mathrm{d}\xi}(\mathrm{Re}(\Xi))\leqslant 1$, $0\leqslant\forall\xi\leqslant\pi$ is a slow operator, denoted by L_s; with $\frac{\mathrm{d}}{\mathrm{d}\xi}(\mathrm{Re}(\Xi))\geqslant 1$, $0\leqslant\forall\xi\leqslant\pi$ is a fast operator; denoted by L_f; with $\exists\pi>\xi_0>0$, $0\leqslant\forall\xi\leqslant\xi_0$, $\frac{\mathrm{d}}{\mathrm{d}\xi}(\mathrm{Re}(\Xi))\geqslant 1$ and $\xi_0\leqslant\forall\xi\leqslant\pi$, $\frac{\mathrm{d}}{\mathrm{d}\xi}(\mathrm{Re}(\Xi))\leqslant 1$ is a mixed operator, denoted by L_m.

According to the classification, a fast operator tends to propagate a wave in a faster speed than the correct speed in the semi-discrete evolution. A slow operator tends to propagate a wave in a slower speed than the correct speed in the semi-discrete evolution. A mixed operator shares the characters of both fast and slow schemes.

1.2 WENO schemes [10,20]

In the WENO method, there are r candidate stencils, each containing r grid points. The one most upwind candidate stencil ranges over mesh point indices $j-(r-1)$ to j, while the fully downwind candidate stencil ranges over j to $j+(r-1)$, and the other candidate stencils fall in between. The final numerical approximation becomes

$$\hat{f}_{j+1/2}=\sum_{l=0}^{r-1}\omega_l\hat{f}_{j+1/2,l}. \tag{7}$$

Specifically, $\hat{f}_{j+1/2,l}$ are rth-order accurate polynomial interplant evaluated at $x_{j+1/2}$. The weights are defined by

$$\beta_k=\sum_{l=0}^{r-1}\int_{x_{j-1/2}}^{x_{j+1/2}}\Delta x^{2l-1}\left(\frac{\mathrm{d}^l\hat{f}}{\mathrm{d}x^l}\right)^2\mathrm{d}x, \tag{8}$$

and

$$\alpha_k=\frac{C_k}{(\beta_k+\varepsilon)^p}, \tag{9}$$

$$\omega_k=\frac{\alpha_k}{\sum_{k=0}^{r-1}\alpha_k}. \tag{10}$$

The small positive number ε prevents division by zero, and p is used to increase or decrease WENO adaptation sensitivity. Details can be found elsewhere [10,20].

2 WGVC

2.1 Two base schemes: mixed and slow operator

We need a fast/mixed scheme and a slow scheme as two base schemes which are used in the two sides of a discontinuity respectively.

In this paper, we use the following $2(r-1)$ order operator with a free parameter

$$L(f_j;\sigma)=\sigma\cdot f_{j-r}+\sum_{l=-(r-1)}^{r-1}a_l(\sigma)\cdot f_{j+l} \tag{11}$$

to obtain the mixed or slow operator. And its numerical flux approaches $h_{j+1/2}=h(x_{j+1/2})$ is

$$\hat{f}_{j+1/2}(\sigma)=\sum_{l=-(r-1)}^{r-1}b_l(\sigma)\cdot f_{j+l}, \tag{12}$$

where the $h(x)$ is implicitly defined as in ref. [21],

$$f(x)=\frac{1}{\Delta x}\int_{x-\Delta x/2}^{x+\Delta x/2}h(\eta)\mathrm{d}\eta. \tag{13}$$

It's evident that the scheme (11) shows different dissipation and dispersion properties when σ chooses different value. According to the GVC theory, a "fast/mixed type" scheme $\hat{f}_{j+1/2}(\sigma_m)$ should be used at the left side of discontinuity and a 'slow type' scheme $\hat{f}_{j+1/2}(\sigma_s)$ must be at the right side of the discontinuity (assume the discontinuity propagates towards right) [18]. The two parameters σ_m and σ_s will be determined in sect. 2.3.

Note that the fifth-order linear upwind scheme (LUW5) and the seventh-order linear upwind scheme (LUW7) are gained when $\sigma=\sigma_0$. That is to say we can get a $2r-1$ order scheme when we choose $\sigma=\sigma_0$. Values of a_l and b_l are listed in Tables 1 and 2, respectively. And values of σ_0 are listed in Table 3.

2.2 Weighted methodology for selection of mixed or slow operator

Consider eq. (1), we propose the following weighted meth-

odology to construct WGVC schemes.

Firstly, we list the two constraints that WGVC schemes should satisfy

(1) The 2(r−1) order mixed scheme $\hat{f}_{j+1/2}(\sigma_m)$ is used behind a discontinuity while the 2(r−1) order slow scheme $\hat{f}_{j+1/2}(\sigma_s)$ is used ahead of the discontinuity.

(2) In the smooth region, the two 2(r−1) order schemes $\hat{f}_{j+1/2}(\sigma_m)$ and $\hat{f}_{j+1/2}(\sigma_s)$ are combined to a scheme of $2r-1$ order, that is, $\hat{f}_{j+1/2}(\sigma_0)=D_m\hat{f}_{j+1/2}(\sigma_m)+D_s\hat{f}_{j+1/2}(\sigma_s)$. Values of the optimal weights D_m and D_s are listed in Table 3.

Secondly, as shown in Figure 1, the whole stencil of the scheme (12) is divided into two disjointed sub-stencils denoted by S_m and S_s.

Calculate the WENO smooth indicators of this two sub-stencils β_m and β_s following eq. (8). Once there is a discontinuity in sub-stencil S_s, this indicates that this point j is behind the discontinuity, thus the mixed scheme $\hat{f}_{j+1/2}(\sigma_m)$ should be used. Similarly, once a discontinuity is in the sub-stencil S_m, it means this point is ahead of the discontinuity, thus the slow scheme $\hat{f}_{j+1/2}(\sigma_s)$ should be used. And the weights of the two sub-stencils are calculated by

$$\gamma_k=\frac{D_k}{\left(\beta_k+\varepsilon\right)^p}, \tag{14}$$

$$\varpi_k=\frac{\gamma_k}{\gamma_m+\gamma_s}, \tag{15}$$

where k=m or s.

The ε is a small positive number which is introduced to prevents division by zero and we use the classical value of ε=10^{-6} as in ref. [10]. The power parameter p is set to 2 as in ref. [10].

Thus we obtain WGVC schemes, that is,

$$\hat{f}_{j+1/2}=\varpi_m\hat{f}_{j+1/2}(\sigma_m)+\varpi_s\hat{f}_{j+1/2}(\sigma_s). \tag{16}$$

Once there is a discontinuity in sub-stencil S_s, the computed weights $\varpi_m\approx 1$, $\varpi_s\approx 0$, thus $\hat{f}_{j+1/2}=\hat{f}_{j+1/2}(\sigma_m)$. Once a discontinuity is in the sub-stencil S_m, the computed weights $\varpi_m\approx 0$, $\varpi_s\approx 1$, then $\hat{f}_{j+1/2}=\hat{f}_{j+1/2}(\sigma_s)$.

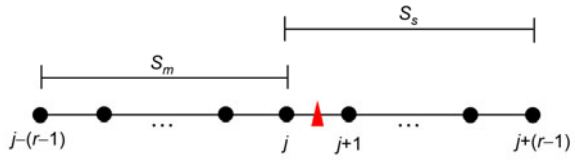

Figure 1 (Color online) Weighted methodology for GVC.

In smooth region, $\hat{f}_{j+1/2}=\hat{f}_{j+1/2}(\sigma_0)$. The two constraints listed above are thus satisfied.

2.3 Determination of σ_m and σ_s

There are two methods to determined the two parameters σ_m and σ_s. One method is the optimization method [22]. For a nonlinear scheme, no analytical formula of the spectral relations can be obtained. However, using the technique suggested by Pirozzoli [23], the approximate dispersion relation (ADR) of the nonlinear scheme still can be obtained. The two parameters σ_m and σ_s can be determined numerically.

The other method is to optimize the shockwave-capturing capability using the one-dimensional Sod shock tube problem [24]. Details can be found elsewhere [18]. In this paper, we use this method and values of the two parameters σ_m and σ_s are listed in Table 3.

In critical points, the WGVC scheme reduce to order of 2(r−1) at most while the WENO scheme reduce to order of r. And the actual ADRs of these nonlinear schemes are shown in sect. 4.1. These results show that WGVC schemes have high-resolution for short waves. In additional, since the WGVC schemes belong to the GVC schemes. they share the moderate shock-capturing capability of the GVC scheme [17,18].

3 Hybrid WGVC-WENO schemes

In this section, we hybrid the WGVC schemes and the WENO schemes of the same order to compute multi-scales flows with discontinuities. The reason are as follows.

The common switch functions usually have artificial parameters. It is easy to adjust the parameters so as to identify less points as discontinuity points. In this situation, the WGVC scheme is used in smooth region (containing some discontinuity points). Thus the problem 'the switch function may mistake some points in smooth waves as discontinuity points, particularly in high-wavenumber waves [15]' can be avoided.

Any switch function can be used. In this paper we use $\theta(s)=s^q\cdot(q+1-q\cdot s)$ as a switch function, where $s=1-\frac{\varpi_m\varpi_s}{D_mD_s}$ and q is a controllable positive integer. Obviously the function θ remains shares: in smooth regions, $\theta\approx 0$; and in discontinuities, $\theta\approx 1$. Extensive numerical tests show the best compromise between accuracy and non-oscillatory properties is ensured for q=100.

4 Numerical tests

In this section, we discuss applications of the WGVC-

WENO schemes for some benchmark cases.

For 1D and 2D compressible fluid problems, the compressible Euler equations are solved in the following manner. The Roe approximation is used for the local characteristic decomposition at the cell faces while the local Lax-Friedriches flux [25] vector splitting is used to split the fluxes into a positive and a negative part, that is, $\boldsymbol{F} = \boldsymbol{F}^+ + \boldsymbol{F}^-$, the new schemes are used in each characteristic fields. After transforming back into physical space, the numerical flux is then obtained. The 3rd-order TVD Runge-Kutta scheme [25] is used for time integration. All computations are carried out with a CFL=0.6.

For 3D tests, the Navier-Stokes equations are solved directly. And the Steger-Warming splitting method is applied while the eight-order central scheme is used to discrete the viscous terms. The others are the same with the 2D tests.

4.1 The spectral properties of WGVC-WENO schemes

In order to show the spectral properties of the proposed WGVC-WENO schemes, their ADRs are plotted in Figures 2 and 3. The spectral properties of the classical WENO schemes [10,20] are also shown for comparison. From Figures 2 and 3, it can be readily seen that the WGVC-WENO schemes show much better resolution for short waves than classical WENO schemes of the same order.

4.2 Shock-density wave interaction

Let us now consider the shock density-wave interaction problem [25]. The initial conditions are set by a Mach 3 shock interacting with a perturbed density filed

$$(\rho, u, p) = \begin{cases} (3.857, 2.629, 10.333), & \text{if } 0 < x < 1, \\ (1 + 0.2\sin(5x), 0, 1), & \text{if } 10 > x > 1. \end{cases}$$

The final time is t=1.8. Note that the "exact" solution is obtained numerical by the classical WENO5 scheme [10] on a grid of 4001 grid points.

Figures 4 and 5 give the computed density profiles calculated by WGVC-WENO5 and WGVC-WENO7 respectively. A agreement with the reference solution is obtained. Due to less numerical dissipation, the results obtained by the WGVC-WENO schemes are heavily improved compared with the WENO schemes of the same order.

Note that the results of this problem are obtained by the WGVC schemes while the WENO schemes are fully turned off. It's obviously the WGVC schemes do share moderate shock-capturing capability.

4.3 Double Mach reflection

Let us now consider the problem of double Mach reflection of a strong shock. A Mach 10 shock wave is reflected form a wall with incident angle of 60°. We set up the problem as given previously [26]. The computation domain of this problem is [0, 0]×[4, 1]. Initially, the shock extends from the point x=1/6 at the bottom to the top of the computational domain. Along the bottom boundary, at y=0, the region from x=0 to x=1/6 is always assigned post-shock conditions, whereas a reflecting wall condition is set from x=1/6 to x=4. Inflow and outflow boundary conditions are applied at the left and right ends of the domain, respectively. The values at the top boundary are set to describe the exact motion of a Mach 10 shock. For this case, the final simulation time is t=0.2.

Figure 6 shows the density contours obtained by WGVC-WENO5 and the classical WENO5 schemes. The contours zoomed around the contact discontinuity and Mach stem region are given in Figure 7. We can clearly see that WGVC-WENO5 resolves better the wave structures near the second triple point and predicts a stronger jet near the wall. As shown in Figure 7, the WGVC-WENO5 resolves considerably finer vertical structure and is less dissipative at small scales.

Figure 8 shows the density contours obtained by WGVC-WENO7 and the classical WENO7 schemes. The contours zoomed around the contact discontinuity and Mach stemregion are given in Figure 9. We can again clearly see that WGVC-WENO7 has almost the same ability to capture

Table 1 Expressions of $a_l(\sigma)$, l=–r, ..., r–1

	a_{-4}	a_{-3}	a_{-2}	a_{-1}	a_0	a_1	a_2	a_3
r=3	–	σ	1/12–5σ	–2/3+10σ	–10σ	2/3+5σ	–1/12–σ	–
r=4	σ	–1/60–7σ	3/20+21σ	–3/4–35σ	35σ	3/4–21σ	–3/20+7σ	1/60–σ

Table 2 Expressions of $b_l(\sigma)$, l=–(r–1), ..., r–1

	b_{-3}	b_{-2}	b_{-1}	b_0	b_1	b_2	b_3
r=3	–	–σ	–1/12+4σ	7/12–6σ	7/12+4σ	–1/12–σ	–
r=4	–σ	1/60+6σ	–2/15–15σ	37/60+20σ	37/60–15σ	–2/15+6σ	1/60–σ

Table 3 Values of σ_{m}, σ_s, σ_0, D_m, D_s

	σ_{m}	σ_{s}	σ_0	D_m	D_s
r=3	–0.07773	0	–1/30	0.42883	0.57117
r=4	0.02205	0	1/140	0.32394	0.67606

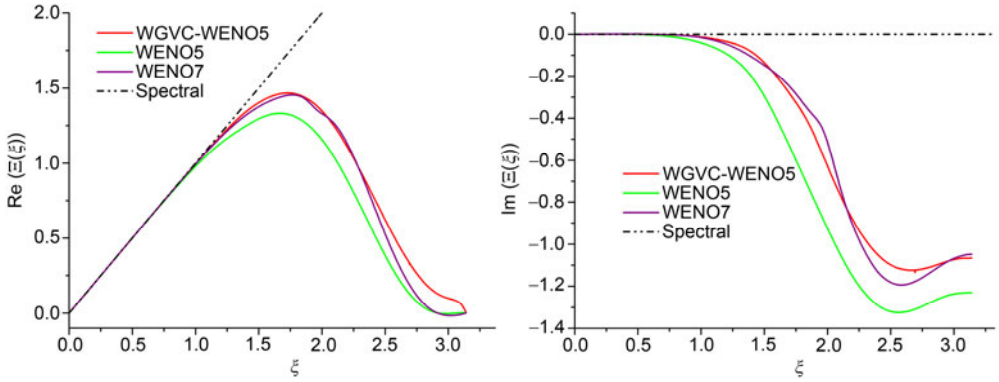

Figure 2 (Color online) Spectral properties of WGVC-WENO5, WENO5 and WENO7.

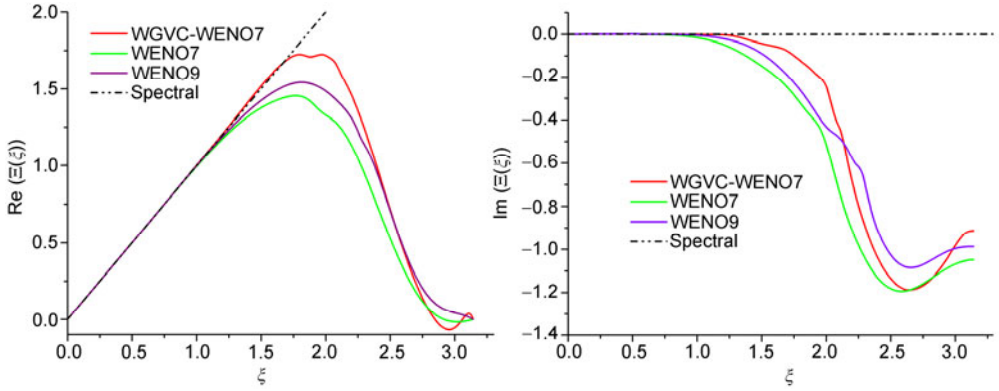

Figure 3 (Color online) Spectral properties of WGVC-WENO7, WENO7 and WENO9.

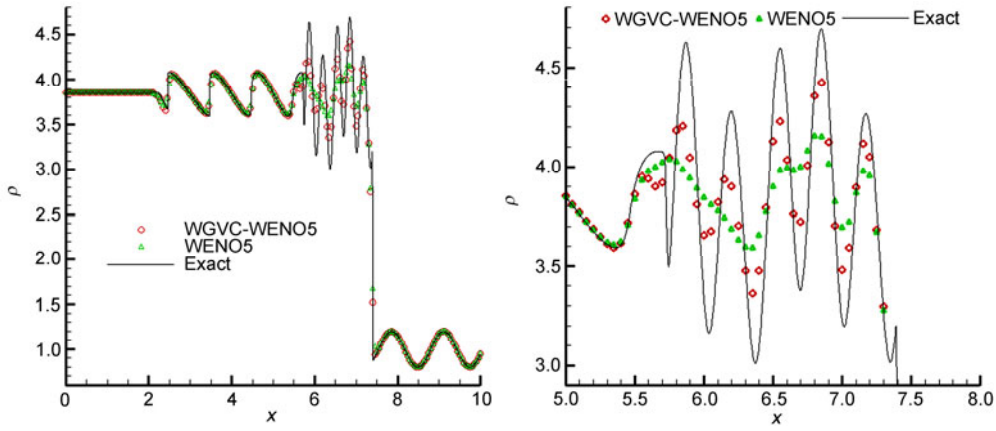

Figure 4 (Color online) Shock-density-wave interaction: density profile on 201 point grid.

strong shock waves as the classical WENO scheme while the resolution of small scales waves is improved again in comparison to the WENO7 scheme.

These tests above show that WGVC-WENO schemes have much better resolution of small scale waves than WENO schemes and fine abilities to capture strong shock waves.

4.4 Rayleigh-Taylor instability

Rayleigh-Taylor instability occurs on an interface between fluids with different densities when acceleration is directed from the heavy fluid to the light fluid. The instability has a fingering nature, with bubbles of light fluid rising into the ambient heavy fluid and spikes of heavy fluid falling into the light fluid [26]. Previous studies show that there are many small scale structures. This can be used as a good example to test the resolution of the numerical schemes. We set up the problem as given previously [26]. The computational domain is [0, 1/4]×[0,1]; initially the interface is at y=1/2, the heavy fluid with ρ=2 is below in the interface, and the light fluid with density ρ=1 is above the interface

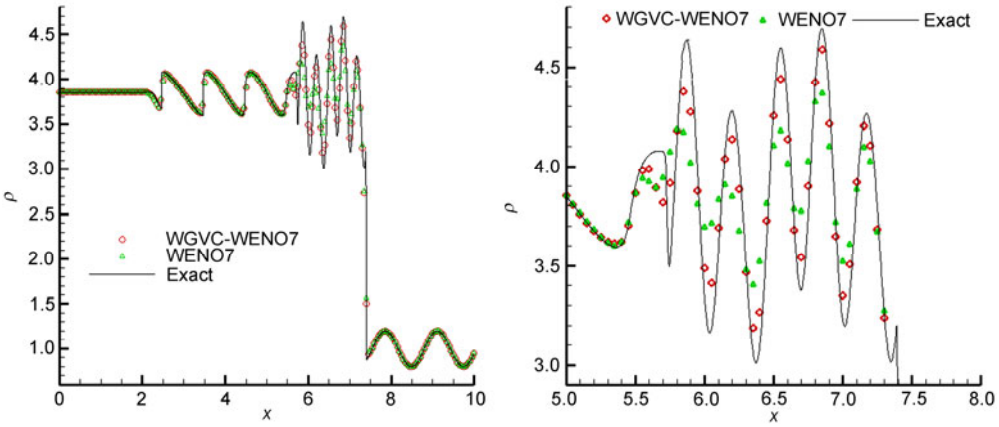

Figure 5 (Color online) Shock-density-wave interaction: density profile on 201 point grid.

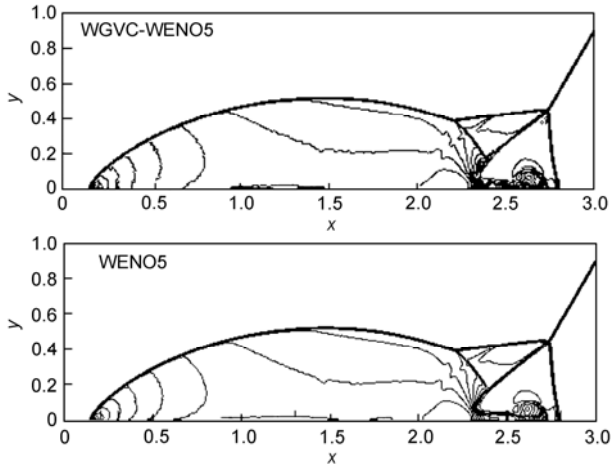

Figure 6 Double-Mach reflection: density profile at t=0.2 on a 961×241 grid. 30 equally spaced contour lines from ρ=1.5 to ρ=22.9705.

with the acceleration in the positive y-direction; the pressure p is continuous across the interface; a small perturbation is given to the velocity component in y direction. Thus, for $0\leqslant y<1/2$, $\rho=2$, $u=0$, $p=2y+1$, $v=-0.025c\cdot\cos(8\pi x)$, and for $1/2\leqslant y\leqslant 1$, $\rho=1$, $u=0$, $p=y+3/2$, $v=-0.025c\cdot\cos(8\pi x)$, where c is the sound speed $c=\sqrt{\gamma p/\rho}$, and the ratio of specific heats γ=5/3. A source term ρ is added to the right hand side of the third equation and ρv is added to the fourth equation of the Euler system. The final simulation time is t=1.95.

Figure 10 shows the density contours obtained by the WGVC-WENO5, WENO5, WGVC-WENO7 and WENO7 schemes on a 121×481 grid. It is apparent that the WGVC-WENO schemes are much less dissipative at small scales than the WENO schemes. We can also observe that the WGVC-WENO schemes can produce more small vortices in the shear layer, indicating that they have better resolution to capture small scale structures. Obviously the WGVC-WENO schemes resolve considerably finer results in comparison to classical WENO schemes.

4.5 DNS of SWTBLI

The interaction of a spatially developing adiabatic turbulent boundary layer at free-stream mach number M_∞=2.3 and Reynolds number $Re_\theta\approx 6370$ (based on the momentum thickness of the upstream boundary layer) with an impinging oblique shock wave (β=32.43°) is performed by means of direct numerical simulation of the compressible Navier-Stoeks equations. This case is designed to mimic the experiment [27].

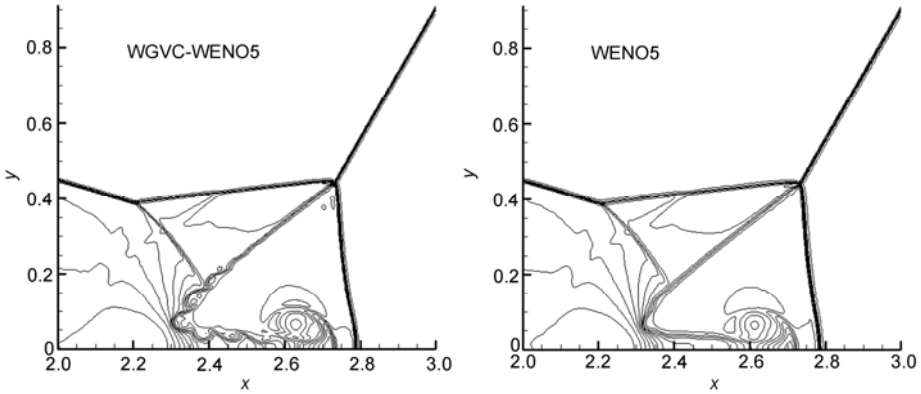

Figure 7 Close-up view of the "blow-up" region of Figure 6. 30 equally spaced contour lines from ρ=1.5 to ρ=22.9705.

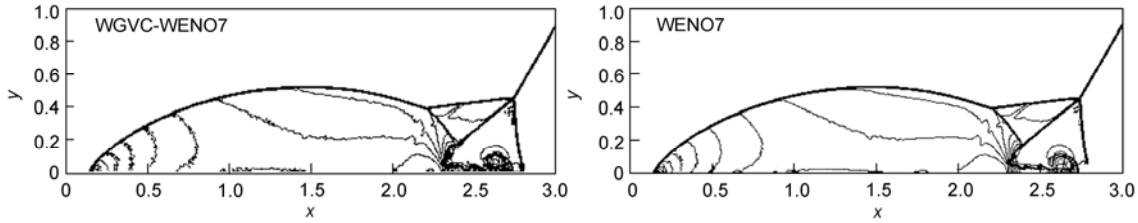

Figure 8 Double-Mach reflection: density profile at t=0.2 on a 961×241 grid. 30 equally spaced contour lines from ρ=1.5 to ρ=22.9705.

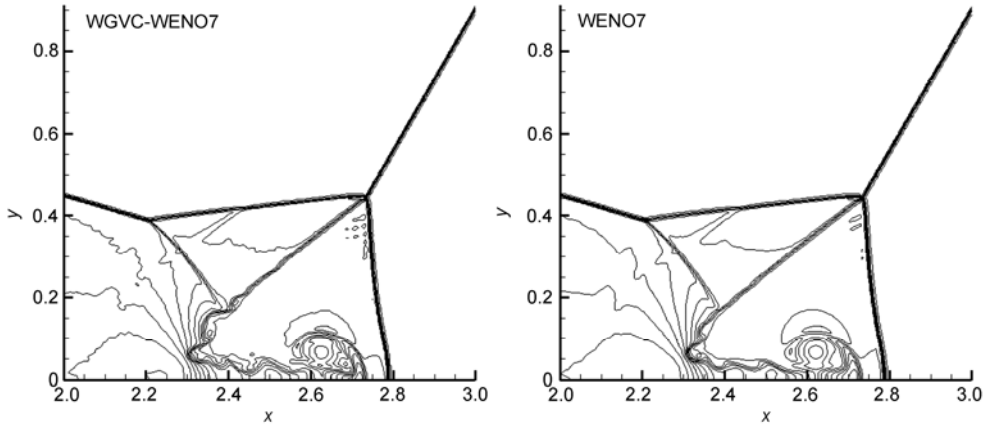

Figure 9 Close-up view of the "blow-up" region of Figure 8. 30 equally spaced contour lines from ρ=1.5 to ρ=22.9705.

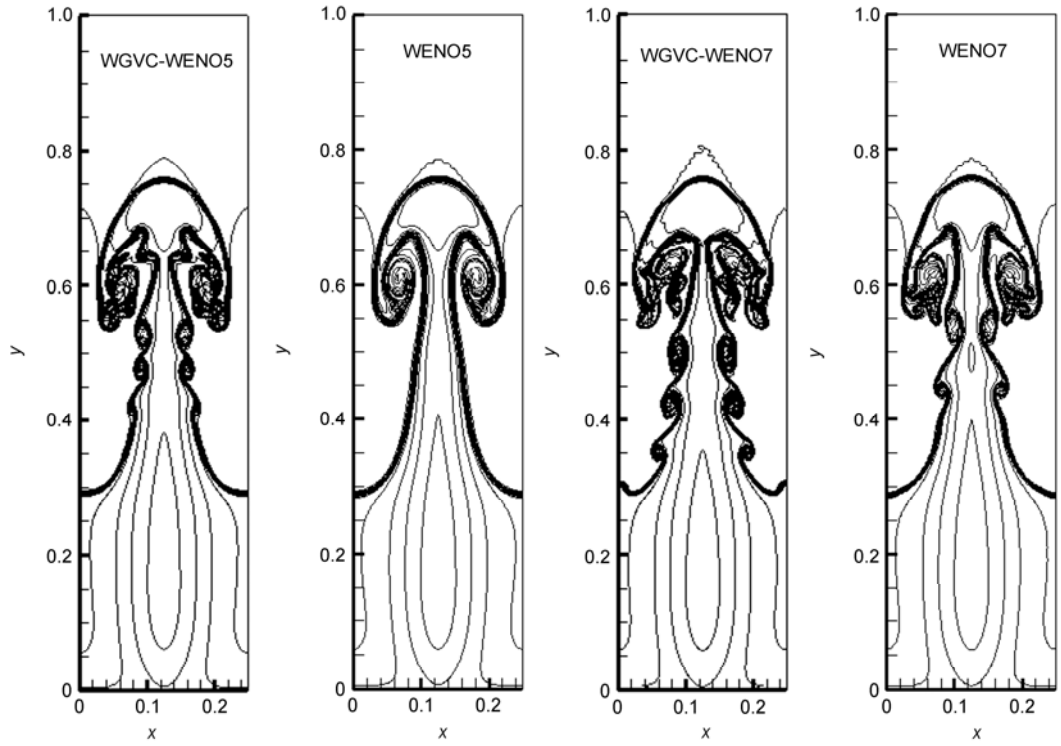

Figure 10 Rayleigh-Taylor Instability: density profile on a 121×481 grid. 15 equally spaced contour lines from ρ=0.952269 to ρ=2.14589.

The computational methodology is as follows: as shown in Figure 11, a time-independent laminar compressible boundary-layer is imposed in inflow boundary. After a long transition, at about x=260 mm, the flow reaches the state of

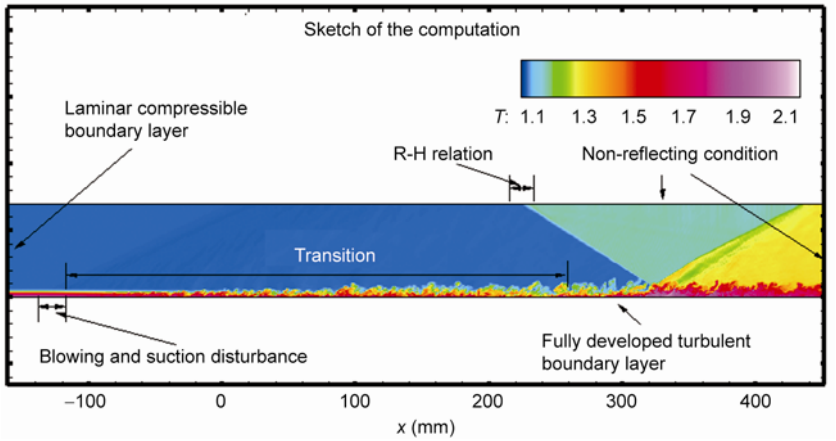

Figure 11 Sketch of the computation.

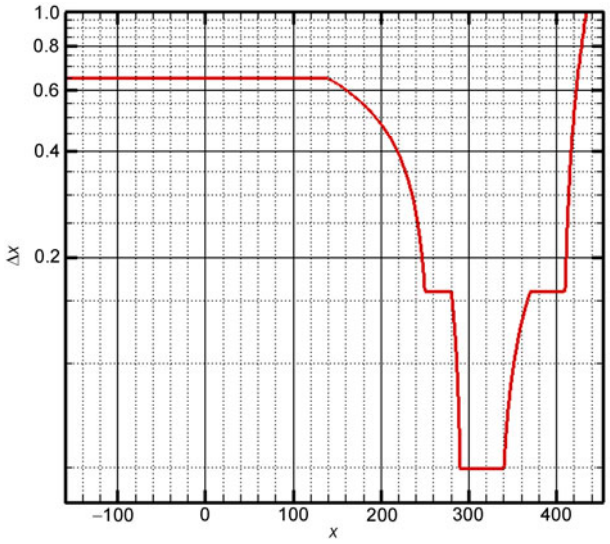

Figure 12 Mesh spacing in the streamwise direction.

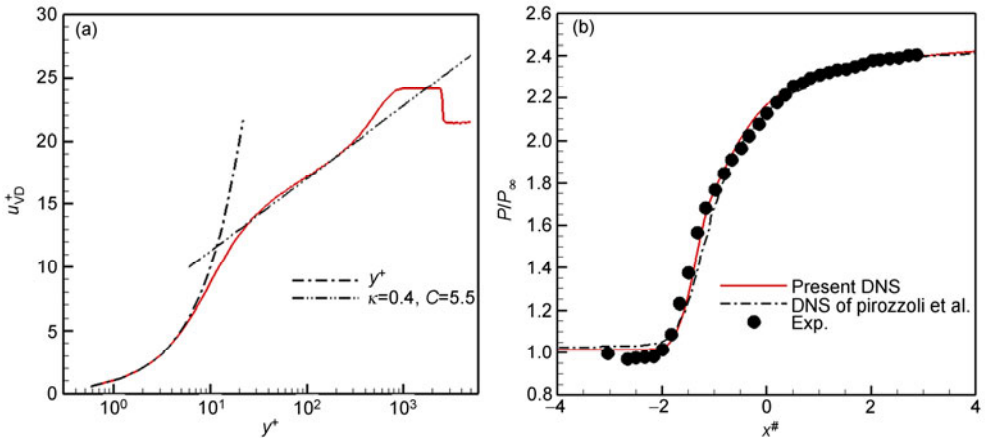

Figure 13 van Driest transformed mean streamwise velocity (a); mean wall pressure (b).

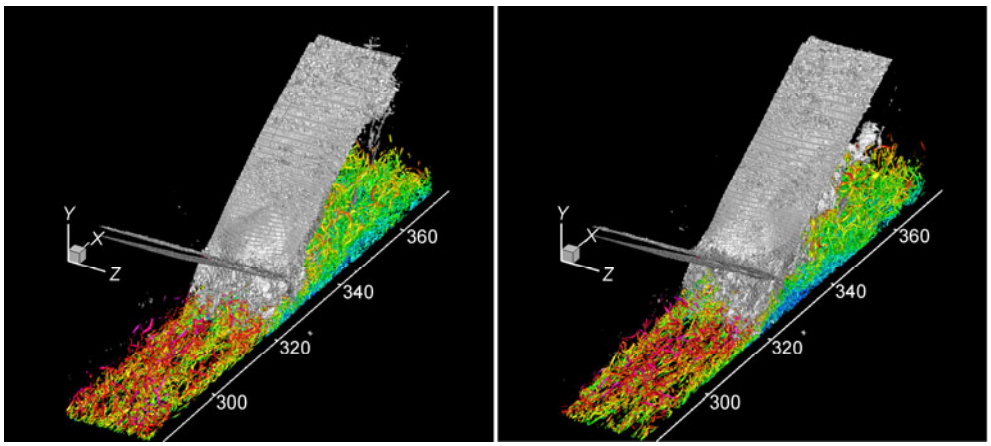

Figure 14 (Color online) The shock system (gray shading) is identified as an isosurface of the modified Ducros sensor.Vortical structures are educed as isosurfaces of Q-criterion and are colored with the local Mach number.

developed turbulence. Concurrently, at the top of the computational domain, and x=225 mm, the Rankine-Hugoniot relations are reinforced, generating an oblique shock wave. A SWTBLI problem is formed as the deduced shock wave impinges the turbulent boundary layer at about x=330 mm. The inviscid flux is discretized by the proposed WGVC-WENO7 scheme.

The grid is 2534×180×256. The computational domain is partitioned into eight zones in the streamwise direction. The mesh spacing in the streamwise direction is shown in Figure 12. In wall normal direction, boundary grid is used and the grid is equally spaced in the spanwise direction. In wall units (based on the boundary layer properties taken at the reference point x=280 mm) the mesh spacings in the streamwise, wall normal, and spanwise directions are $\Delta x^+_{\min}\times\Delta y^+_{\min}\times\Delta z^+ = 3.80\times0.57\times4.21$.

Figure 13(a) shows the van Driest velocity profile at the reference point of the upstream boundary layer, that is, x=280 mm. We can see the log region can be described by $(1/\kappa)\log(y^+)+C$, with κ=0.4 and C=5.5. The streamwise wall mean pressure profile is given in Figure 13(b) which shows good quantitative agreement with the experimental results, in which $x^{\#}=(x-x_{\text{imp}})/L$ where x_{imp} is the mean location of the extension of the impinging shock to the wall and $L=x_{\text{imp}}-x_{\text{sep}}$ in which x_{sep} is the mean boundary layer separation location. Note the DNS data of Pirozzoli et al. [28] whose conditions are sufficiently close to the experiment we have selected are also presented.

In Figure 14, the shock system (gray shading) is identified as an isosurface of the modified Ducros sensor [29]. Vortical structures are educe as isosurfaces of Q-criterion [30] and are colored with the local mach number. We show two instantaneous flow fields at two different times. We can see that the reflected shock experiences spanwise perturbations which are well captured using the proposed WGVC-WENO7 scheme.

5 Conclusions

One problem in spectral-like resolution-WENO hybrid schemes is: if the switch function takes more grid points as discontinuity points, the WENO scheme is often turned on, and the numerical solutions may be too dissipative. Conversely, if the switch function takes less grid points as discontinuity points, the hybrid schemes usually are found to produce oscillatory solution or just to be unstable.

To correct this problem we suggest the following method. If the spectral-like resolution scheme in the hybrid scheme has moderate shock-capturing capability, the final hybrid scheme is inclined to be more stable, even the switch function takes less grid points as discontinuity points.

Following this idea, we propose a new class of nonlinear schemes named WGVC schemes. These schemes show high-resolution for short waves and moderate shock-capturing capability. Then a new class of hybrid schemes is designed in which WGVC scheme is used in the smooth region and WENO scheme is used to capture discontinuities. These hybrid schemes show good resolution for small-scales structures and fine shock-capturing capabilities. The seven-order WGVC-WENO scheme has also been applied successfully to the DNS of oblique SWTBLI.

Thanks to Profs. FU DeXun and MA YanWen for helpful discussions. This work was supported by the National Natural Science Foundation of China (Grant Nos. 11372330 and 11072248), the National High Technology Research and Development Program of China (Grant No. 2012AA01A304) and the Chinese Academy of Sciences Program (Grant Nos. KJCX2-EW-J01 and XXH12503-02-02-04). The authors thank National Supercomputer Center in Tianjin (NSCC), Supercomputing Center of Chinese Academy of Sciences (SCCAS) and Shanghai Supercomputer Center (SSC) for providing computer time.

1 Dolling D S. Fifty years of shock-wave/boundary-layer interaction research: What next? AIAA J, 2001, 39: 1517–1531
2 Sun Z S, Ren Y X, Larricq C, et al. A class of finite difference

schemes with low dispersion and controllable dissipation for DNS of compressible turbulence. J Comput Phys, 2011, 230(12): 4616–4635
3 Fu D X, Ma Y W. A high order accurate difference scheme for complex flow fields. J Comput Phys, 1997. 134(1): 1–15
4 He Z W, Li X L, Fu D X, et al. A 5th order monotonicity-preserving upwind compact difference scheme. Sci China-Phys Mech Astron, 2011, 54(3): 511–522
5 Tam C K W, Webb J C. Dispersion-relation-preserving finite difference schemes for computational acoustics. J Comput Phys, 1993, 107: 262–281
6 Li Y. Wavenumber-extended high-order upwind-biased finite difference schemes for convective scalar transport. J Comput Phys, 1997, 133: 235–255
7 Lele S K. Compact finite difference schemes with spectral-like resolution. J Comput Phys, 1992, 103: 16–42
8 Honein A E, Moin P. Higher entropy conservation and numerical stability of compressible turbulence simulations. J Comput Phys, 2004, 201(2): 531–545
9 Kim S, Lee S, Kim K H. Wavenumber-extended high-order oscillation control finite volume schemes for multi-dimensional aeroacoustic computations. J Comput Phys, 2008, 227(8): 4089–4122
10 Jiang G S, Shu C W. Efficient implementation of weighted ENO schemes. J Comput Phys, 1996, 126: 202–228
11 Ren Y X, Liu M E, Zhang H. A characteristic-wise hybrid compact-WENO scheme for solving hyperbolic conservation laws. J Comput Phys, 2003, 192: 365–386
12 Adams N A, Shariff K. A high-resolution hybrid compact-ENO scheme for shock-turbulence interaction problems. J Comput Phys, 1996, 127(1): 27–51
13 Pirozzoli S. Conservative hybrid compact-WENO schemes for shock-turbulence interaction. J Comput Phys, 2003, 178: 81–117
14 Kim D, Kwon J H. A high-order accurate hybrid scheme using a central flux scheme and a WENO scheme for compressible flowfield analysis. J Comput Phys, 2005, 210: 554–583
15 Zhou Q, Yao Z, He F, et al. A new family of high-order compact upwind difference schemes with good spectral resolution. J Comput Phys, 2007, 227(2): 1306–1339
16 Fu D X, Ma Y W, Kobayashi T. Nonphysical oscillations in numerical solutions: Reason and improvement. Comput Fluid Dyn J, 1996, 4: 427–450
17 Ma Y, Fu D X. Fourth order accurate compact scheme with group velocity control (GVC). Sci China Ser A, 2001, 44(9): 1197–1204
18 Li X, Fu D, Ma Y. Optimized group velocity control scheme and DNS of decaying compressible turbulence of relative high turbulent Mach number. Int J Numer Meth Fluids, 2005, 48(8): 835–852
19 Trefethen L N. Group velocity in finite-difference schemes. SIAM Rev, 1982, 24(2): 113–136
20 Balsara D S, Shu C W. Monotonicity preserving weighted essentially non-oscillatory schemes with increasingly high order of accuracy. J Comput Phys, 2000, 160: 405–452
21 Shu C W, Osher S. Efficient implementation of essentially non-oscillatory shock-capturing schemes. J Comput Phys, 1988, 77: 439–471
22 Martín M P, Taylor E M, Wu M, et al. A bandwidth-optimized WENO scheme for the effective direct numerical simulation of compressible turbulence. J Comput Phys, 2006, 220: 270–289
23 Pirozzoli S. On the spectral properties of shock-capturing schemes. J Comput Phys, 2006, 219: 489–497
24 Sod G A. A survey of several finite difference methods for systems of non-linear hyperbolic conservation laws. J Comput Phys, 1978, 27: 1–31
25 Shu C W, Osher S. Efficient implementation of essentially non-oscillatory shock-capturing schemes, II. J Comput Phys, 1989, 83: 32–78
26 Shi J, Zhang Y T, Shu C W. Resolution of high order WENO schemes for complicated flow structures. J Comput Phys, 2003, 186: 690–696
27 Dupont P, Haddad C, Debiève J F. Space and time organization in a shock-induced separated boundary layer. J Fluid Mech, 2006, 559: 255–277
28 Pirozzoli S. Grasso F. Direct numerical simulation of impinging shock wave/turbulent boundary layer interaction at M=2.25. Phys Fluids, 2006, 18(6): 065113
29 Pirozzoli S, Numerical methods for high-speed flows. Annu Rev Fluid Mech, 2011, 43: 163–194
30 Hunt J C R, Way A, Moin P. Eddies, stream, and convergence zones in uurbulent flows. Center for Turbulence Research Report CTR-S88 (1988), 1988